Patient Safety Starts with **Independence.**

With ever-increasing imaging and treatment variables, an independent approach to Quality Management ensures safety is never taken for granted.

At Sun Nuclear, we deliver proven independent QA solutions for Radiation Therapy and Diagnostic Imaging. More than 5,000 hospitals and clinics worldwide count on us to help:

- Mitigate errors
- Reduce inefficiencies
- Validate technologies and techniques
- Elevate clinical care

For user insights, key publications and product updates, **visit sunnuclear.com.**

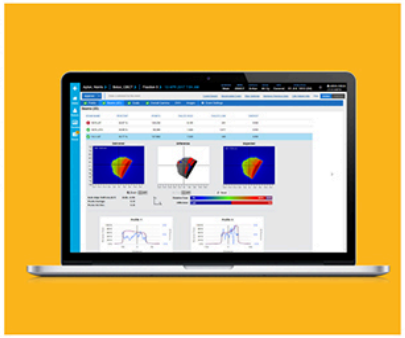

SUN NUCLEAR corporation

Patient Safety Starts Here

Respiratory-gated CT as a tool for the simulation of breathing artifacts in PET and PET/CT

J. J. Hamill[a)]
Siemens Medical Solutions, Knoxville, Tennessee 37932

G. Bosmans and A. Dekker
Department of Radiation Oncology (MAASTRO), GROW, University Hospital Maastricht, Maastricht, The Netherlands

(Received 6 July 2007; revised 6 December 2007; accepted for publication 6 December 2007; published 23 January 2008)

Respiratory motion in PET and PET/CT blurs the images and can cause attenuation-related errors in quantitative parameters such as standard uptake values. In rare instances, this problem even causes localization errors and the disappearance of tumors that should be detectable. Attenuation errors are severe near the diaphragm and can be enhanced when the attenuation correction is based on a CT series acquired during a breath-hold. To quantify the errors and identify the parameters associated with them, the authors performed a simulated PET scan based on respiratory-gated CT studies of five lung cancer patients. Diaphragmatic motion ranged from 8 to 25 mm in the five patients. The CT series were converted to 511-keV attenuation maps which were forward-projected and exponentiated to form sinograms of PET attenuation factors at each phase of respiration. The CT images were also segmented to form a PET object, moving with the same motion as the CT series. In the moving PET object, spherical 20 mm mobile tumors were created in the vicinity of the dome of the liver and immobile 20 mm tumors in the midchest region. The moving PET objects were forward-projected and attenuated, then reconstructed in several ways: phase-matched PET and CT, gated PET with ungated CT, ungated PET with gated CT, and conventional PET. Spatial resolution and statistical noise were not modeled. In each case, tumor uptake recovery factor was defined by comparing the maximum reconstructed pixel value with the known correct value. Mobile 10 and 30 mm tumors were also simulated in the case of a patient with 11 mm of breathing motion. Phase-matched gated PET and CT gave essentially perfect PET reconstructions in the simulation. Gated PET with ungated CT gave tumors of the correct shape, but recovery was too large by an amount that depended on the extent of the motion, as much as 90% for mobile tumors and 60% for immobile tumors. Gated CT with ungated PET resulted in blurred tumors and caused recovery errors between −50% and +75%. Recovery in clinical scans would be 0%−20% lower than stated because spatial resolution was not included in the simulation. Mobile tumors near the dome of the liver were subject to the largest errors in either case. Conventional PET for 20 mm tumors was quantitative in cases of motion less than 15 mm because of canceling errors in blurring and attenuation, but the recovery factors were too low by as much as 30% in cases of motion greater than 15 mm. The 10 mm tumors were blurred by motion to a greater extent, causing a greater SUV underestimation than in the case of 20 mm tumors, and the 30 mm tumors were blurred less. Quantitative PET imaging near the diaphragm requires proper matching of attenuation information to the emission information. The problem of missed tumors near the diaphragm can be reduced by acquiring attenuation-correction information near end expiration. A simple PET/CT protocol requiring no gating equipment also addresses this problem. [DOI: 10.1118/1.2829875]

Key words: respiration, gating, PET, CT, tumor, numerical simulation

I. INTRODUCTION

Accurate measurement of tumor standard uptake values (SUV) is an important requirement in many PET applications. In whole-body PET studies SUV is believed to be an indicator of tumor avidity and a predictor of patient survival rates[1–4] and accurate quantitation is important when autodelineation is used in therapy planning.[5–8] Indeed, an important requirement for PET in oncology is to detect every tumor that is large enough and has enough tracer uptake to be detectable. Respiratory motion is one factor with the potential to reduce quantitative accuracy and to cause missed or misplaced tumors near the diaphragm. For example, the report by Keall *et al.* shows that significant motion is observed in many regions of significance to oncology[9] and the report by Osman *et al.* indicates the possibility of localization and detection errors near the diaphragm.[10] In the state of the art, however, PET and PET/CT reconstruction algorithms are based on the assumption that the patient does not move during the measurement of the emission sinogram and the attenuation factors (AF).

Motion causes two phenomena which lead to image artifacts. First, the tracer distribution moves, blurring the image. Second, the AFs change with time, leading to too much or too little correction for attenuation on some lines of response. The latter problem is severe near the diaphragm and is sometimes enhanced when the AFs are based on a CT series acquired during a breath-hold, with the associated problem that lesions in fusion images of CT and PET could be mislocated, e.g., from the liver into the lung.[10,11] One goal of this article is to indicate clearly, in the case of PET tumor imaging, what kinds of error arise from respiratory motion in conventional PET (CP), considering the complicated interplay between these two sources of error.

Another goal of this article is to demonstrate the advantages of respiratory gating in acquisition of the PET or AF information.[12–14] We are interested in respiratory-gated PET (GP), in respiratory-gated CT (GCT), in PET/CT performed with attenuation measurements from nongated CT, in nongated PET/CT with gated CT, and in PET/CT in which both modalities are gated. Practical problems are associated with clinical and phantom-based investigations of the benefits of gating. One problem is the low statistics in each phase of GP. Another problem is that laboratory studies are likely to use an unrealistic model of the breathing seen in patients. In this article, we avoid those problems by using GCT as the basis for a simulated PET emission data set, created with a digital computer. To our knowledge such a simulation has not yet been reported in the literature. A preliminary version of this work was presented earlier.[15]

This approach can address the following issues. How well does conventional PET do in the presence of such motion? Does the answer depend strongly on the location or size of the tumor that is affected by motion? Is phase matching of GP and GCT quantitative? Does GP or GCT by itself solve the motion problem, delivering a quantitative result? What PET/CT imaging protocols, based on technology available today, minimize respiration-related errors?

II. METHODS

Our investigation is derived from a set of five GCT studies of lung cancer patients, selected at random from the population of patients receiving GCT at the Maastro Clinic. Although this is a small number of patients, the extent of breathing motion in this set covers much of the range seen in patients[9,19] and results in a large body of information about six tumor locations in five patients, that is, 30 positions in all. Patients' breathing was monitored by a strain gauge worn around the abdomen.[16] Low-pitch helical CT scans of the chest were performed with a 16-slice CT scanner (Sensation 16, Siemens AG, Forchheim, Germany). The data for the five patients were retrospectively reconstructed into images representing a 500 mm field of view sampled by a 512×512 matrix, with 3 mm between slices, and ten phases of the respiration cycle starting at end inspiration. GCT images were converted to a map $\mu(\vec{b},r)$ of PET attenuation coefficients[17] at each phase of respiration r and image location $\vec{b}$. These were transformed to a sinogram of AF values at those phases by applying a high-resolution forward projector[18] then rebinned to 168 radial and 168 angular bins. Our equation for this is

$$\mathrm{AF}(\vec{d},r)=\exp(-R\{\mu(\vec{b},r)\}), \tag{1}$$

where R is the Radon transform and $\vec{d}$ represents a sinogram bin. Related to this quantity is the average attenuation, which, if the patient's breathing pattern were perfectly regular, would be the same as the AF in a high-quality scan in a PET attenuation scan with transmission sources. For us the defining equation in the case of ten gates is

$$\mathrm{AF}(\vec{d})=\frac{1}{10}\sum_{r}\mathrm{AF}(\vec{d},r). \tag{2}$$

This equation, like [Eq. (7)] below, reflects an assumption that a sum over ten sampled values is a good approximation of the underlying integral over the time interval associated with the gate, averaging all the motion during the interval. Other related quantities are the sinogram of attenuation correction factors (ACF) in each gate

$$\mathrm{ACF}(\vec{d},r)=\frac{1}{\mathrm{AF}(\vec{d},r)}, \tag{3}$$

and the ACF corresponding to the average attenuation

$$\mathrm{ACF}(\vec{d})=\frac{1}{\mathrm{AF}(\vec{d})}. \tag{4}$$

The CT series were also segmented to form a simulated PET volume in which a solitary tumor could be imbedded. The PET volumes were defined through a segmentation procedure whose parameters were determined by studying typical whole-body PET/CT studies. First, to enable a smooth segmentation, we reduced CT image noise by smoothing three dimensionally with a Gaussian kernel whose full width at half maximum was 3 mm. Next, the segmentation procedure was run. Pixels with CT numbers between −25 and 200 HU, representing soft tissue and marrow, were assigned a SUV of 1.0. Pixels between −300 and −25 HU (fat) were assigned SUV=0.3. Pixels between −950 and −300 (lung) were assigned SUV=0.17. Pixels above 200 HU (bone) were assigned SUV=0.1. This procedure had several unrealistic characteristics. For example, the blood in the ventricles of the heart was treated like soft tissue and clothing and blankets were sometimes treated like fat.

By inspecting coronal and sagittal sections through the sequence of image volumes of each of the five patients, we located the dome of the liver (DOL) in each phase of respiration. This was always possible, though there were cases in which a tumor sat near the DOL so that the interface between liver and lung was obscured. We used a model in which the motion of the DOL was entirely in the superior/inferior (SI) direction, the most common direction of tumor motion in the survey of Keall *et al.*[9] and in the study by Liu *et al.*[19] We simulated a solitary tumor in one of six places: three mobile tumors were simulated on the right side and three immobile ones in the midchest. The mobile ones were assigned a po-

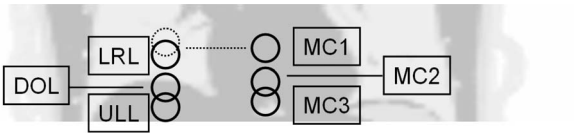

FIG. 1. Coronal section through a segmented PET object based on patient 2 at end inspiration. Solid circles indicate the locations of simulated tumors. Abbreviations refer to lower right lung, dome of the liver, upper lobe of the liver, and midchest positions 1, 2, and 3. The dotted circle shows the lower right lung lesion at end expiration, 11.1 mm higher in this patient. The dotted line shows the respiration-averaged position of the lower-right-lung lesion.

sition relative to the DOL position in each gate. Each simulated tumor, mobile or immobile, was assumed to be spherical in shape and filled uniformly with radioactivity, with an assigned SUV=5.0 and a diameter of 10, 20, or 30 mm. A mobile tumor denoted DOL was centered 5 mm below the DOL position. A mobile tumor denoted LRL was defined 25 mm higher than the DOL tumor, in the lower right lung, that is, 20 mm above the dome of the liver. A mobile tumor denoted ULL was defined 15 mm below the DOL tumor, in the upper lobe of the liver. The three immobile tumors were placed in the midchest and were denoted MC1, MC2, and MC3. Their SI coordinates were set equal to the mean positions of the mobile LRL, DOL, and ULL tumors, respectively. The six tumor locations are indicated by Fig. 1.

The voxelized PET volume in each gate r and voxel $\vec{b}$ is denoted $O(\vec{b},r)$, We transformed these into unattenuated two-dimensional (2D) sinograms, $p_{\text{no att}}(\vec{d},r)$, using the forward projector referred to above, again with 168 radial and 168 angular samples. The equation for this is

$$p_{\text{no att}}(\vec{d},r) = R\{O(\vec{b},r)\}. \tag{5}$$

Attenuated 2D PET sinograms were made by multiplying the PET sinograms by the AF sinograms

$$p(\vec{d},r) = \text{AF}(\vec{d},r) \times p_{\text{no att}}(\vec{d},r). \tag{6}$$

These would be the sinograms measured by a PET scanner with respiratory gating, apart from effects such as limited spatial resolution, scattered radiation, and spatial sensitivity variations. Those effects were not included in the simulation, so that the study could focus exclusively on effects due to motion. We also were interested in the time-averaged sinogram, defined as

$$p(\vec{d}) = \frac{1}{10}\sum_r p(\vec{d},r). \tag{7}$$

Seven types of PET volume were extracted for analysis and comparison. The first of these was $O(\vec{b},r)$, described above. Second was the time average of these, denoted

$$O(\vec{b}) = \frac{1}{10}\sum_r O(\vec{b},r). \tag{8}$$

Third was the series derived by reconstructing the gated sinograms with attenuation correction derived from the matched CT gate. These were made with filtered backprojection according to the equation

$$I_{\text{GP-GCT}}(\vec{b},r) = R^{-1}\{p(\vec{d},r) \times \text{ACF}(\vec{d},r)\}, \tag{9}$$

where R^{-1} is the inverse Radon transformation. Although iterative reconstruction is now the usual reconstruction method in whole-body PET,[20,21] filtered backprojection is appropriate in the absence of statistical noise because it is a gold standard and because there is no question of when to stop the iterations. With the exceptions defined by Eqs. (13) and (14) below, we did not blur the reconstructed images to give a clinical level of spatial resolution.

The fourth PET series to be compared was derived by reconstructing gated sinograms with the average attenuation. This series was associated with the respiratory gate index used for PET reconstruction. It represents, under the assumption of regular breathing, what is achievable when gated PET is used on a PET scanner with a conventional measurement of the attenuation, i.e., a 511-keV transmission scan with rotating rods of ^{68}Ge. The defining equation is

$$I_{\text{GP}}(\vec{b},r) = R^{-1}\{p(\vec{d},r) \times \text{ACF}(\vec{d})\}. \tag{10}$$

Similarly, the fifth PET series to be compared was obtained when the emission sinograms were time averaged, i.e., not gated, but the CT was gated. The PET series was associated with the respiratory gate index of the CT that was used for AC. Considering this data set, one can ask whether a particular state of respiration can be used for attenuation correction. Also, we can investigate what happens when the free-breathing patient is imaged with a very fast CT scan at an arbitrary state of respiration. The defining equation for this case is

$$I_{\text{GCT}}(\underline{b},r) = R^{-1}\{p(\vec{d}) \times \text{ACF}(\vec{d},r)\}. \tag{11}$$

Conventional PET was the sixth PET series to be compared. In this case, both the emission and attenuation were time averaged. Again operating under the assumption that one breathing cycle is the same as a long time average, we have the following defining equation:

$$I_{\text{CP}}(\vec{b}) = R^{-1}\{p(\vec{d}) \times \text{ACF}(\vec{d})\} = \frac{1}{10}\sum_r I_{\text{GP}}(\vec{b},r). \tag{12}$$

The seventh, final type of PET image to be compared was the GCT image based on CT acquired at EE or EI. In these cases, and these cases only, we attempted to model the spatial resolution of state-of-the-art PET scanners. Our equations for these images are

$$I_{\text{GCT-EE}}(\vec{b}) = I_{\text{GCT}}(\vec{b},r)|_{r=\text{EE}} \otimes g(\vec{b}) \tag{13}$$

and

$$I_{\text{GCT-EI}}(\vec{b}) = I_{\text{GCT}}(\vec{b},r)|_{r=EI} \otimes g(\vec{b}), \tag{14}$$

where the symbol $\otimes$ represents convolution and g is a three-dimensional Gaussian kernel, whose full width at half maxi-

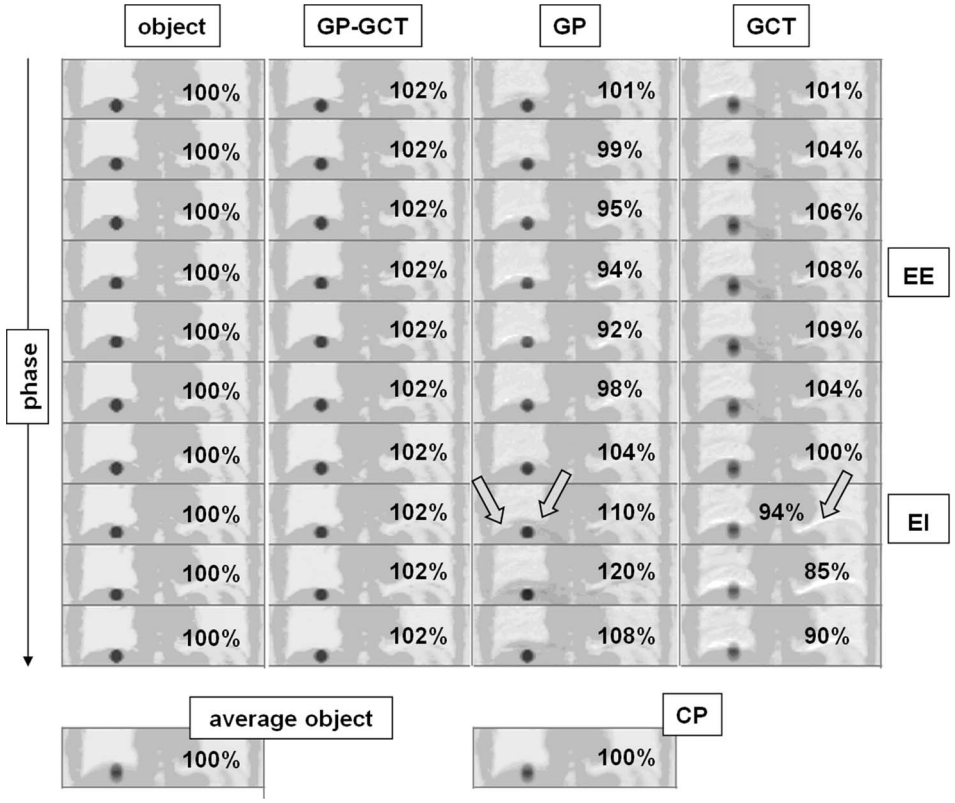

FIG. 2. Coronal sections through PET series associated with the 20 mm dome of the liver tumor in patient 4. The figure presents the PET object at each gate, the average object, three gated reconstructed image sequences, and a nongated reconstruction, as explained in the text. SUV recovery is indicated with a percent value in each frame of the picture. Arrows indicate prominent artifacts. Abbreviations refer to gated PET, gated CT, conventional PET, end expiration, and end inspiration.

mum was set to 6.4 mm to represent 4 mm instrument resolution and 5 mm smoothing to reduce image noise.

We analyzed each of these PET volumes in three ways, based on a maximum-intensity coronal projection over a 10 mm coronal slice that contained the tumor. First, the SUV of the tumor was defined as the maximum pixel value in the coronal slice containing the tumor. We converted this to a percent recovery figure by dividing by the expected SUV value (the value is 5.0) and multiplying by 100. This maximum-pixel method, and related methods based on regions around the maximum, are used commonly in clinical PET and PET/CT.[1–4] Second, the image of the tumor itself was inspected to see if the correct shape was obtained in the reconstruction. A round shape of the same diameter as the lesion (10, 20, or 30 mm) was expected. Third, the image of the surrounding tissues was inspected visually for artifacts.

Because there were in principle three tumor diameters, six locations, five patients, and ten phases of respiration, this procedure should lead to the creation of 900 simulated PET volumes to be processed in our study. We reduced the magnitude of our study by first fixing the tumor diameter at 20 mm and considering the range of motion and positions seen in five patients and six tumor locations, then studying effects related to the tumor's size by considering mobile tumors in one patient.

III. RESULTS

III.A. The diaphragmatic motion model

The motion of the DOL in our model is characterized in each patient and at each phase of respiration by a single value, the z coordinate used to simulate the positions of the mobile tumors. The total excursions in z (and the root mean square) for the five patients, ranked from least motion to most motion, were: patient 1, 8.4 mm (2.8 mm); patient 2, 11.1 mm (3.4 mm); patient 3, 13.8 mm (4.3 mm); patient 4, 19.8 mm (5.4 mm); and patient 5, 25.2 mm (8.5 mm).

Patients 3 and 5 had actual large tumors in the lower right lung. In both cases, the diaphragm could be visualized in sagittal and coronal sections, allowing us to define the DOL unambiguously. In both cases, our methodology placed the simulated LRL tumor inside these actual masses. The other three patient studies had no such large masses in the lower right lung.

III.B. Typical images in the case of 20 mm tumors

Figure 2 presents coronal sections through $O(\vec{b},r)$, $O(\vec{b})$, $I_{\text{GP-GCT}}(\vec{b},r)$, $I_{\text{GP}}(\vec{b},r)$, $I_{\text{GCT}}(\vec{b},r)$, and $I_{\text{CP}}(\vec{b})$ for patient 4, in the case where we simulated a tumor at the DOL. The figure also indicates which phases represent end expiration (EE)

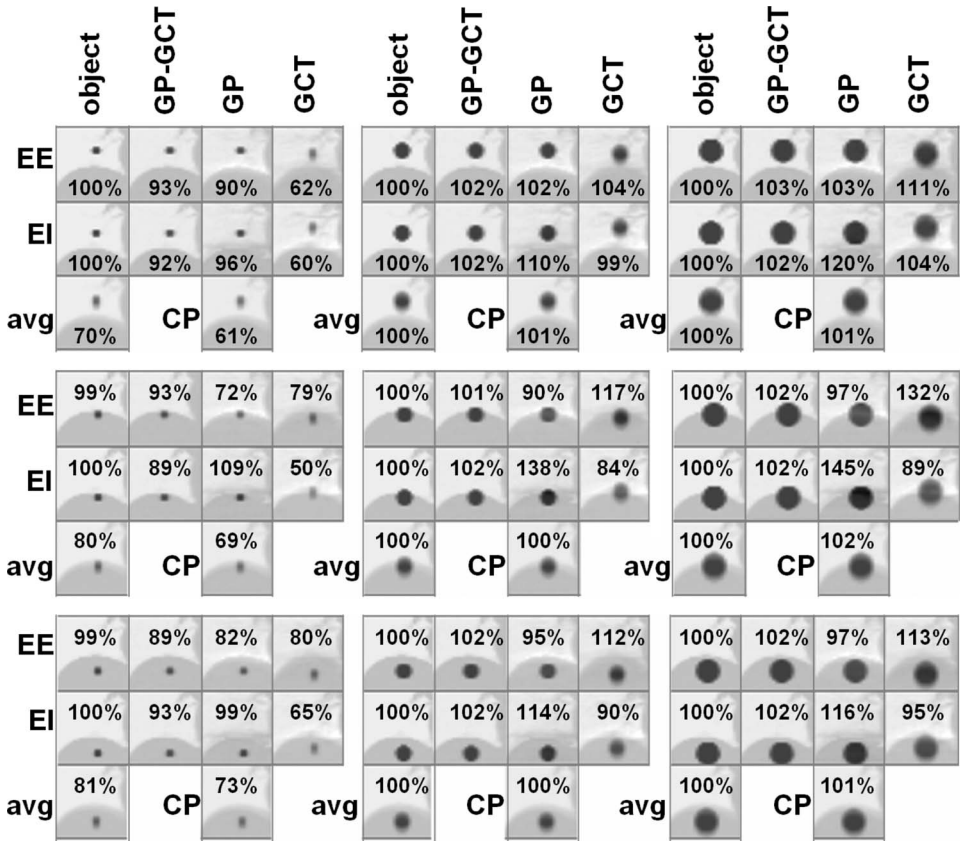

FIG. 3. Coronal sections through PET series associated with mobile 10, 20, and 30 mm tumors in patient 2, at end expiration (EE) and end inspiration (EI), the average (avg), and conventional PET (CP). The top three rows of the figure show tumors in the lower right lung. Middle: at the dome of the liver. Bottom: in the upper lobe of the liver. The left four rows: 10 mm tumors. Middle: 20 mm. Right: 30 mm. Percentages printed in the figure are SUV recovery values.

and end inspiration (EI). The percent recovery of the lesion SUV in each position is printed in each frame of the picture.

In this simulation, the phase-matched reconstructions (GP-GCT) produced correct SUV recovery and created no striking artifacts. Actually, recovered values were in most cases 1%–2% too high because of reconstruction noise.

Figure 2 also indicates that the recovery varied from phase to phase when one used the GP and GCT methods. This is discussed in the following sections. Reconstruction artifacts were evident when one used either of those methods. They were particularly noticeable near the diaphragm. These are indicated with arrows in Fig. 2.

III.C. Typical images for 10, 20, and 30 mm tumors

We had simulated 10, 20, and 30 mm lesions in our earlier analysis[15] of patient 5. Since then we have also simulated 10, 20, and 30 mm tumors in patient 2, who had no tumor in the lower lung and whose breathing excursion was a more typical amount, 11.1 mm. Figure 3 presents images of the simulated mobile tumors in the three positions of interest, at EE and EI, for all three tumor sizes. The same attenuation-correction methods are used as in Sec. III B. The percent recovery of SUV is printed in each frame of the picture.

III.D. Motion blurring and SUV recovery

The motion-blurring phenomenon is best studied by examining the time-averaged simulated tumor, $O(\vec{b})$. One would expect that respiration should blur edges in the object, and this was borne out by our study of the diaphragm image in $O(\vec{b})$, for example the average object in the bottom left corner of Fig. 2. The tumor's image was distended and blurred in the SI direction. Also, the diaphragm's sharp edges were replaced with diffuse ones. In $O(\vec{b})$, the tumor uptake determined as the maximum pixel was 100% in the mobile tumors in patients 1, 2, 3, and 4, where the motion was less than the tumor diameter, but uptake was between 69% and 73% in patient 5, where the motion exceeded the tumor diameter.

Figure 4 illustrates the blurring of the moving tumors. The figure shows the 20 mm tumors at the dome of the liver in patient 2, who had 11.1 mm of respiratory motion, and patient 5, who had 25.2 mm of motion. The figure compares EE and EI and includes a comparison with the time-averaged object and the CP reconstruction. One will notice a slight flattening at the edges of the sphere, due to our use of a voxel model in which the separation between slices was 3 mm.

The figure shows that phase-matched PET/CT, represented by the GP-GCT images, was in principle capable of

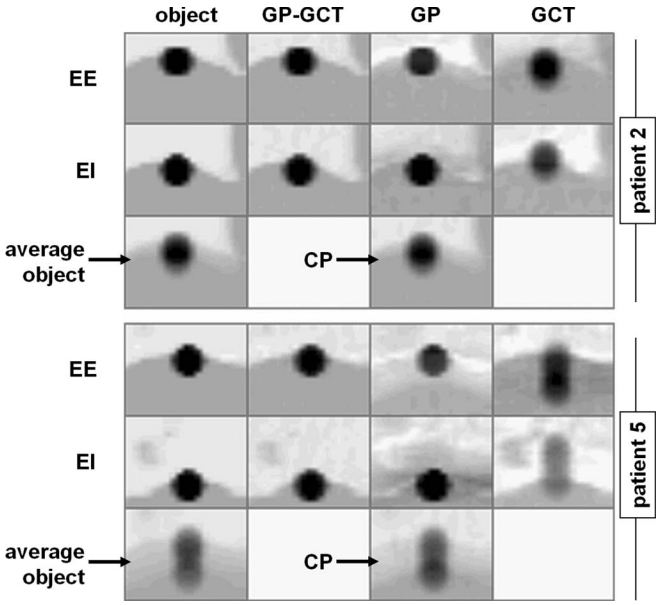

FIG. 4. Coronal section through a simulated 20 mm tumor in patients 2 and 5 at the dome of the liver, at respiratory phases EE and EI. Averages are also shown. Abbreviations refer to gated PET, gated CT, conventional PET, end expiration, and end inspiration.

generating an essentially perfect replica of the object itself at each phase of respiration. The tumor had the correct shape and was uniformly filled with the correct values. The surrounding tissues were also reproduced well. When the PET was gated but the CT was not, the shape of the tumor was correct but the distribution of activity inside the tumor was nonuniform and SUV values in the surrounding tissues were wrong. When the CT was gated and the PET was not, the tumor was distorted and the background values were in error. Conventional PET, in these examples, gave nearly the same image as motion blurring alone.

Considering all six tumor locations in patients 1, 2, and 3, who had less than 15 mm of breathing motion, and all ten phases of respiration, we found the range of values shown in Table I. GP-GCT always gave essentially 100% recovery. In the case of GP, the largest error (overestimation of the recovery) occurred at or near EI and the most negative error (underestimation) occurred at or near EE.

We also present the recovery values for patients 4 and 5, who had more than 15 mm of motion. These are summarized in Table II.

We calculated the SUV recovery for all six tumors reconstructed by the GCT method at EE and EI, with Gaussian filtering included, according to Eqs. (13) and (14). The recovery values are plotted in Fig. 5 as a function of the amount of diaphragmatic motion.

IV. DISCUSSION

A quantitative PET or PET/CT reconstruction procedure requires compensation for the physical effects that distinguish the actual measurement from an ideal measurement based on unattenuated line integrals of the radioactivity density. Those effects include photon attenuation, statistical fluctuations, a background of scattered radiation, random coincidences, positron range effects, noncolinearity in the two annihilation photons, detector sensitivity variations, and patient motion. In oncological PET, attenuation is normally the largest of these effects, with attenuation factors sometimes in excess of 100 in abdominal and shoulder sections but about an order of magnitude less than that in lung sections. At the level of the diaphragm, this largest effect changes from moment to moment with the patient's breathing. Motion of the radioactive tracer in internal organs is also an important effect in this region in the breathing patient. At the outset of this investigation, it seemed to us that an understanding of the effect of breathing upon PET's accuracy in this anatomical region should include a realistic model of the diaphragm's actual motion in cancer patients. Respiratory-gated CT made this possible, providing measurements of the anatomy of the entire chest.

Our study of respiratory motion effects in PET/CT was driven by GCT series from five patient studies. The range of diaphragmatic motion in this set of five studies was from 8 to

TABLE I. Range of SUV recovery for 20 mm lesions in patients 1, 2, and 3 who had less than 15 mm of breathing motion. The average value is presented if the range is less than 5%. The values reported in the table are the smallest and largest recovery values in these three patients, considering all phases of respiration. Abbreviations refer to gated PET, gated CT, conventional PET, the lower right lung, the dome of the liver, the upper lobe of the liver, and three positions in the midchest.

	GP-GCT (%)	GP (%)	GCT (%)	CP (%)
Mobile				
LRL	102	100–110	97–109	101
DOL	101	93–145	90–122	100
ULL	102	94–114	94–112	100
Immobile				
MC1	102	99–108	97–119	102
MC2	102	97–111	99–112	101
MC3	102	92–115	93–120	101

TABLE II. Range of SUV recovery for 20 mm lesions in patients 4 and 5 who had more than 15 mm of breathing motion. The average value is presented if the range is less than 5%. The values reported in the table are the smallest and largest recovery values in these two patients, considering all phases of respiration. Abbreviations refer to gated PET, gated CT, conventional PET, the lower right lung, the dome of the liver, the upper lobe of the liver, and three positions in the midchest.

	GP-GCT (%)	GP	GCT	CP
Mobile				
LRL	102	100–158	68–106	70–89
DOL	101	92–191	45–120	76–100
ULL	101	73–134	55–108	72–101
Imobile				
MC1	102	100–108	100–108	101
MC2	102	85–164	91–130	102
MC3	102	85–189	78–175	102

25 mm, with three of the five cases showing motion less than 15 mm. This range of motion is typical of the range seen in a number of clinics around the world.[9,19] We considered 10, 20, and 30 mm tumors. First we asked, how well did various image-reconstruction approaches work for a given tumor size, considering a variety of locations and breathing patterns? Second, we asked, how do the results change in the case of mobile tumors of three different sizes? In the remainder of this section, we will address these questions in turn, then consider the clinical significance of the findings.

IV.A. SUV recovery for 20 mm tumors

In our simulation of 20 mm tumors, shown for example in Fig. 2, the combination of gated PET with gated CT provided accurate results for each patient and each tumor location at every phase of respiration. This indicated that the Radon transform of the PET object, generated by our forward projector, was correctly inverted by our filtered backprojection algorithm. This was a reassuring check on the correctness of the computational tools that we used.

Gating of the PET alone gave the correct tumor shape but was not quantitative. Gating of the CT alone gave a shape like the shape caused by motion blur alone and was not quantitative. This was also true of conventional PET. A PET/CT study performed using a CT scan of a free-breathing patient should be similar to gated CT with a random choice of the respiratory phase, provided that the CT scan is performed rapidly enough, i.e., it unavoidably has the same kinds of errors as ungated PET with GCT. A PET/CT study with a CT scan at deep inspiration cannot be modeled by our simulation, since the position of the diaphragm is likely to be outside the range seen in the PET scan of a freely breathing patient.

The case of an immobile tumor with no background activity is an important limit. In this limit, the time-averaged attenuation correction given by [Eq. (4)] is exact and CP should be as accurate as GP-GCT. One can speculate that CP should also be nearly quantitative when the tumor is immobile and the background is small but not zero. Further, CP might be nearly quantitative when the motion is less than the tumor size. This prediction is confirmed by the bottom three rows of Tables I and II, which show that both GP-GCT and CP gave SUV recovery of nearly 100%. However, GP and GCT are not quantitative, with errors less than 20% for motion less than 15% but larger errors in the case of more motion.

The mobile tumors were more susceptible to quantitation errors because they were motion-blurred and also subject to attenuation errors. Tables I and II show that GP-GCT was accurate in every case. CP was more accurate than either GP or GCT in the imaging of mobile 20 mm tumors, although CP underestimated the SUV by about 30% in the case of patient 5 with 25 mm of motion. The tables show that the GP and GCT methods are not quantitative. More motion causes larger errors in SUV recovery.

When respiration moves a tumor by more than the diameter of the tumor, no PET or PET/CT reconstruction method can be expected to recover the tumor's actual SUV values, unless the method accounts for the motion. In our simulation of this case, no part of the tumor at EE overlapped the tumor at EI. On the other hand, if in our simulation the total motion was less than the diameter, the bottom of the tumor at EE overlapped the top of the tumor at EI. Since we assumed that the uptake was uniform throughout the tumor, this situation creates the illusion that a piece of the tumor did not move. Because we focused our attention on 20 mm tumors, and because SUV values were assigned based on maximum pixel values, motion less than 15 mm had relatively little effect.

The poorest SUV recovery was for tumors close to the dome of the liver. We believe that this was due to large changes, over the course of the respiratory cycle, in attenuation values. The upper lobe of the liver was also strongly influenced by attenuation changes, though the effect was less than at the DOL. Quantitative errors in the lower right lung were generally of a smaller magnitude and we believe are mostly due to motion-blurring alone, with much smaller attenuation errors. An exception occurred in the case of the LRL tumor in patient 4 with the GP method, when gating near EI placed the lower part of the tumor well inside the time-averaged shadow of the diaphragm. At that respiratory phase the tumor was perfectly round, but attenuation correction gave an SUV recovery value as large as 158%.

IV.B. SUV recovery for 10, 20, and 30 mm tumors in one patient

Although this research focused on 20 mm tumors, in Sec. III B we considered mobile 10, 20, and 30 mm tumors in patient 2, in whom the breathing motion was 11.l mm. The results are summarized by Fig. 3.

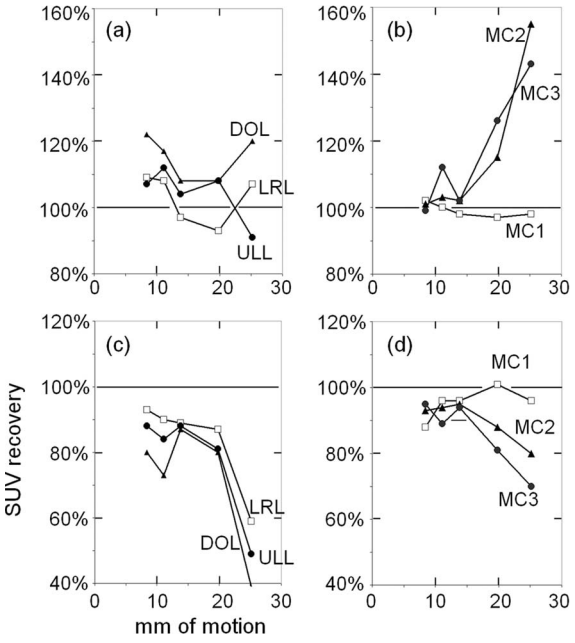

FIG. 5. SUV recovery for 20 mm tumors measured with nongated PET, reconstructed with [(a), (b)] CT at end expiration and [(c), (d)] CT at end inspiration. Six tumor locations are reported: [(a), (c)] lower right lung, dome of the liver, and upper lobe of the liver; and [(b), (d)] positions 1, 2, and 3 in the midchest.

In the case of 10 mm tumors, the average object was blurred by the motion, causing a 20%–30% reduction in SUV recovery. The GP-GCT combination, which worked well in our simulation of 20 mm tumors, recovered about 90% of the correct SUV in this case. The small error was a partial-volume effect due to the voxel model and to the lack of smoothing as a part of image reconstruction. In our simulation, GP and GCT reconstructions each caused small SUV recovery errors if the gating was taken at EE or EI, depending on the tumor location. An actual reconstruction of this case would suffer from further SUV reductions due to scanner resolution, smoothing during reconstruction, and other effects not included in the simulation.

The 30 mm tumors were more accurately imaged than the 20 mm ones. The GP-GCT combination worked perfectly in this case. When the GP or GCT methods were used, SUV recovery errors were too high or too low by 20%–30%. Close inspection shows that the hottest pixels occurred in a small region of the tumor where attenuation errors were greatest, for example near the diaphragm, so the overestimations of SUV recovery would be less than this in an actual PET scan, because the additional blurring of an actual PET scan was not modeled.

IV.C. Clinical significance

In many clinics where oncological PET/CT is performed today, the PET data are not gated and a CT scan is performed without special equipment or breathing instructions that would assure data acquisition at a particular, measured phase of breathing.

In the case of a freely breathing patient, the phase most likely to be measured by the spiraling x-ray source is EE because people normally pause between breaths, though the data could be acquired at any phase between EE and EI. We gave special consideration to those two extremes and in Fig. 5 plotted SUV recovery for 20 mm tumors as a function of the extent of the five patients' diaphragmatic motion. In these cases we included a postreconstruction filter to give a more realistic estimate of the recovery achievable in an actual PET/CT scanner, considering spatial resolution. The partial volume effects reduced uptake between 0% and 10%.

Figure 5(a) shows that, in the absence of PET gating, an attenuation correction derived at EE gives good SUV recovery in the case of mobile 20 mm tumors, even when the magnitude of breathing is large. Attenuation correction derived at EI results in underestimation that gets more and more serious as the amount of breathing increases. In fact, the motion blurring is large in both cases. The comparatively good recovery in Fig. 5(a) is actually due to canceling errors: underestimation due to motion blurring and overestimation due to attenuation.

Figures 5(b) and 5(d) show the uptake recovery of immobile 20 mm tumors. In Sec. IV A we pointed out that the average attenuation [Eq. (4)] should give the correct result, yet Fig. 5 shows that the MC1 tumor had nearly perfect SUV recovery, whether the attenuation was derived from EE or from EI. This is because the EE and EI attenuation corrections are nearly the same as the average attenuation. The attenuation changed only a little with respiration because the MC1 tumor location was above the shadow cast by the diaphragm. On the other hand, the immobile MC2 and MC3 tumors, lower in the chest, were in the moving shadow of the diaphragm. Figure 5 shows that attenuation correction based on EE [Fig. 5(b)] caused an overestimation of SUV whereas the correction based on EI [Fig.(d)] causes an underestimation.

Goerres *et al.* have studied the problem of choosing an appropriate breathing protocol for nongated PET/CT, arguing that there are advantages to measuring the attenuation at normal expiration.[22,23] Our methods allow one to study this point of view, since this is the same as GCT at the EE phase. The discussion of the last two paragraphs indicates that EE often works well, but can break down in the case of 20 mm immobile tumors just below the diaphragm. Sections III C and IV B demonstrate that motion blur in nongated PET is a source of inaccuracy in the case of small tumors, even when EE is used for the attenuation correction.

Gated CT is relatively new technology, made practical by the introduction of ever faster CT scanners with large numbers of detector rows. In our methodology for simulating a PET/CT acquisition and reconstruction system with breathing motion, gated CT volumes were converted into PET volumes and attenuation sinograms to represent the essential features of respiratory motion. This approach to studying respiration artifacts in PET/CT has benefits not easily achieved in other approaches, for example clinical studies and phantom studies. First, this approach has a gold standard, since one always compares the tumors to the known tumor introduced in the simulation. Clinical studies hardly ever have such a gold standard to compare to. Second, the motions are realistic since they come from actual patients. In our view, it would be very difficult to create phantom studies in which the motions are modeled with this level of realism. Since actual human tissue is used in our model of the attenuation correction, this approach even includes complex attenuation-related phenomena such as the compression of lung tissue during breathing. Third, we are able to explore the effect of respiratory motion without the confusion of other effects that are present in actual PET studies: limited counts per acquired frame, limits to the detector resolution, three-dimensional instead of two-dimensional geometry, scattered radiation, and other data corrections. When we want to study motion in isolation from other effects, it is advantageous to be able to turn them off.

Our segmentation procedure had some unrealistic features. Blood in the ventricles of the heart was treated like soft tissue and clothing and blankets were sometimes treated like fat. These problems do not concern us greatly, for two reasons. First, the unrealistic effects did not occur close to the lung lesions, where the motion-related effects were large. Second, we believe that the fundamental lessons of the simulation do not depend on objects in the background.

The simulation had other unrealistic features. The spherical shape of the tumors is a logical choice for a first study by a new simulation methodology, but it is hardly realistic. Car-

diac motions in the same territory as the diaphragm pose a separate problem that this simulation did not address.

The respiratory gates were defined at ten equally spaced intervals in the respiratory cycle. A correct physical description of the PET and AF acquisitions would involve integration over all breaths. If we assume a regular and smooth pattern of breathing, the addition of ten phases is nearly the same as time integration, in the sense that a Riemann integral can be approximated with the trapezoid rule. Our model completely ignores motion within each gate. We are not concerned by this because time integration of the motion in such a short frame, which is the appropriate physical model, is well approximated by the average value which we used, given the smooth nature of normal breathing.

The GP-GCT combination gave quantitative PET images in conditions of no statistical noise and under the assumption that the two modalities can be matched perfectly. Clinically, none of the conditions of this simulation can be met realistically. Challenges for the future include finding ways of matching the two modalities well enough to achieve quantitative accuracy in essentially every scan, especially in the presence of variable breathing patterns,[24,25] and finding ways to improve the statistical accuracy of images based on very low statistics per frame.

Actual tumors are irregularly shaped, not spherical. In some clinics, a tumor's SUV is determined by drawing an irregular region over the most intense area of FDG accumulation and evaluating the hottest 90% of the pixels in the region.[3] This procedure could be applied in the case of the spherical shape we assumed. The procedure would agree with our methodology when resolution is good and the hot region is confined to a small part of the tumor, as it did in our study in cases of artifacts near the dome of the liver, where just a part of the tumor appeared very hot. In cases in which the resolution is not good, for example when filtering is applied in order to control image noise, this procedure would tend to reduce the SUV recovery from the values we have presented. That is, the overestimations would be less severe and the underestimations more so.

This simulation can be used to guide practitioners of oncological PET/CT to make the best possible use of existing technology in the face of respiration-related artifacts. The mismatch between the CT and PET images leads to a number of potential problems, including localization and attenuation correction errors. Particularly when a tumor is near the diaphragm in the base of the lungs or in the superior portion of the liver, respiration may result in incorrect localization or even in the tumor being missed because of the undercorrection for attenuation. Fortunately, in a study by Osman *et al.*, the incidence of mispositioning errors was small (less than 2% of cases).[10] Nevertheless, careful attention should be given when reviewing the region near the diaphragm. The review should include PET images made without attenuation correction. Although those images are not quantitative, they are unaffected by attenuation correction errors. In the case of cooperative patients, undercorrection of attenuation due to breathing can be avoided by acquiring the CT scan of the thorax near EE. For patients who are unable to follow breathing instructions, the technologist can acquire two or three fast, low-dose CT scans during free breathing.[26] The appropriate CT scan for attenuation correction, i.e., the one that most closely corresponds to EE, is identified as the one in which the diaphragm is positioned highest. Such a procedure should reduce the likelihood that tumors near the diaphragm are missed because of respiration artifacts and would be particularly appropriate for mobile tumors. For stationary tumors, our work indicates that quantitative imaging is more accurate when the attenuation information is derived near EI. A multi-CT protocol like the one mentioned above can also be used to select the scan in which the diaphragm is lowest. This is the breathing phase proposed by Nehmeh *et al.* for tumor imaging.[11] Therefore, existing technology provides several strategies for tumor imaging in the region near the diaphragm.

V. SUMMARY

We used a gated CT series to provide a realistic basis for simulating errors in PET and PET/CT that are due to respiratory motion. To our knowledge this has not been done previously.

We showed that, in the conditions of the simulation, the combination of gated PET and gated CT was quantitative but other methods were not. In the majority of patients whose breathing motions are less than 15 mm, motion-related errors are in the range of 20% or less in the case of 20 mm tumors. Conventional PET was not quantitative, but there were a remarkable number of cases in our simulation of 20 mm tumors, indeed, nearly all of them, in which canceling errors due to emission blurring and attenuation overestimation led to a nearly correct result in conventional PET, for example in Fig. 2.

We showed that a large amount of motion caused relatively large errors for the 20 mm tumors. The 10 mm tumors that we also simulated in a limited context were blurred to a greater extent by motion. Quantitative imaging of such small tumors is in any case challenged by spatial-resolution effects, which could be larger than the motion blurring, depending on processing parameters. Conversely, 30 mm tumors were blurred less by motion. We demonstrated that gated PET by itself gave the correct shape for tumors, but without proper attenuation information gated PET could not be relied upon to give a quantitative image of the tumor.

The largest uptake errors occurred in tumors at the diaphragm. The upper lobe of the liver was another region where large errors occurred. The lower lung was a territory where uptake errors were smaller in most cases, presumably because the attenuation-correction errors are less while the motion blurring was the same.

Although proper alignment of the emission and transmission measurements is necessary for accurate tumor imaging near the diaphragm, the serious problem of a missed tumor can be addressed without respiratory gating, using simple CT protocols to acquire images near end expiration. By using such a protocol, tumor SUV values are overestimated by an

amount in the range from 0% to 60%. In cases of suspected tumors near the diaphragm, the physician should review the PET images made without attenuation.

ACKNOWLEDGMENTS

This work arose out of discussions with Dr. T. Pan at the M. D. Anderson Cancer Center, who shared gated CT image sets with us and performed related calculations. Our understanding of the imaging of moving tumors was aided by discussions with Dr. D. Townsend and Dr. C. Nahmias at the University of Tennessee and with our colleagues Dr. C. Michel, Dr. B. Bendriem, and Dr. L. Le Meunier. The suggestion to use multiple CT scans of the chest to identify end expiration came from our cardiac PET/CT collaboration with Dr. R. Eisner and Dr. R. Patterson at Emory Crawford Long Hospital.

[a]Electronic mail: james.hamill@siemens.com

[1]G. R. Borst and J. S. Belderbos, "R. Boellaard R, E. F. I. Comans, K. De Jaeger, A. A. Lammertsma, J. V. Lebesque, "Standardised FDG uptake: A prognostic factor for inoperable non-small cell lung cancer," Eur. J. Cancer **41**, 1533–1541 (2005).

[2]S. M. Eschmann, G. Friedel, F. Paulsen, M. Reimold, T. Hehr, W. Budach, J. Scheiderbauer, H. J. Machulla, H. Dittmann, R. Vonthein, and R. Bares, "Is standardised ^{18}F-FDG uptake value an outcome predictor in patients with stage III non-small cell lung cancer?" Eur. J. Nucl. Med. Mol. Imaging **33**, 263–269 (2006).

[3]K. Higashi, Y. Ueda, Y. Arisaka, T. Sakuma, Y. Nambu, M. Oguchi, H. Seki, S. Taki, H. Tonami, and I. Yamamoto, "^{18}F-FDG uptake as a biologic prognostic factor for recurrence in patients with surgically resected non-small cell lung cancer," J. Nucl. Med. **43**, 39–45 (2002).

[4]J. F. Vansteenkiste, S. G. Stroobants, P. J. Dupont, P. R. De Leyn, E. K. Verbeken, G. J. Deneffe, L. A. Mortelmans, and M. G. Demedts, "Prognostic importance of the standardized uptake value on ^{18}F-fluoro-2-deoxy-glucose-positron emission tomography scan in non-small-cell lung cancer: An analysis of 125 cases," J. Clin. Oncol. **17**, 3201–3206 (1999).

[5]A. van Baardwijk, G. Bosmans, L. Boersma, J. Buijsen, S. Wanders, M. Hochstenbag, R. J. vanSuylen, A. Dekker, C. Dehing-Oberije, R. Houben, S. M. Bentzen, M. van Kroonenburgh, P. Lambin, and D. De Ruysscher, "PET-CT based auto-contouring in non-small cell lung cancer correlates with pathology and reduces interobserver variability in the delineation of the primary tumor and involved nodes," Int. J. Radiat. Oncol. Biol. Phys. **68**, 771–778 (2007).

[6]I. S. Grills, D. Yan, Q. C. Black, C. O. Wong, A. A. Martinez, and L. L. Kestin, "Clinical implications of defining the gross tumor volume with combination of CT and ^{18}FDG-positron emission tomography in non-small-cell lung cancer," Int. J. Radiat. Oncol. Biol. Phys. **67**, 709–719 (2007).

[7]Y. E. Erdi, O. Mawlawi, S. M. Larson, M. Imbriaco, H. Yeung, R. Finn, and J. L. Humm, "Segmentation of lung lesion volume by adaptive positron emission tomography image thresholding," Cancer **80**, 2505–2509 (1997).

[8]U. Nestle, S. Kremp, A. Schaefer-Schuler, C. Sebastian-Welsch, D. Hellwig, C. Rübe, and C. M. Kirsch, "Comparison of different methods for delineation of ^{18}F-FDG PET-positive tissue for target volume definition in radiotherapy of patients with non-small cell lung cancer," J. Nucl. Med. **46**, 1342–1348 (2005).

[9]P. J. Keall, G. S. Mageras, J. M. Balter, R. S. Emery, K. M. Forster, S. B. Jiang, J. M. Kapatoes, D. A. Low, M. J. Murphy, B. R. Murray, C. R. Ramsey, M. B. Van Herk, S. S. Vedam, J. W. Wong, and E. Yorke, "The management of respiratory motion in radiation oncology report of AAPM Task Group 76," Med. Phys. **33**, 3874–3900 (2006).

[10]M. M. Osman, C. Cohade, Y. Nakamoto, L. T. Marshall, J. P. Leal, and R. L. Wahl, "Clinically significant inaccurate localization of lesions with PET/CT: Frequency in 300 patients," J. Nucl. Med. **44**, 240–243 (2003).

[11]S. A. Nehmeh, Y. E. Erdi, G. S. P. Meirelles, O. Squire, S. M. Larson, J. L. Humm, and H. Schöder, "Deep-inspiration breath-hold PET/CT of the thorax," J. Nucl. Med. **48**, 22–26 (2007).

[12]C. C. Nagel, G. Bosmans, A. L. A. J. Dekker, M. C. Öllers, D. K. M. De Ruysscher, P. Lambin, A. W. H. Minken, N. Lang, and K. P. Schäfers, "Phased attenuation correction in respiration correlated computed tomography/positron emitted tomography," Med. Phys. **33**, 1840–1847 (2006).

[13]J. W. H. Wolthaus, M. van Herk, S. H. Muller, J. S. A. Belderbos, J. V. Lebesque, J. A. de Bois, M. M. G. Rossi, and E. M. F. Damen, "Fusion of respiration-correlated PET and CT scans: Correlated lung tumour motion in anatomical and functional scans," Phys. Med. Biol. **50**, 1569–1583 (2005).

[14]Y. E. Erdi, S. A. Nehmeh, T. Pan, A. Pevsner, K. E. Rosenzweig, G. Mageras, E. D. Yorke, H. Schoder, W. Hsiao, O. D. Squire, P. Vernon, J. B. Ashman, H. Mostafavi, S. M. Larson, and J. L. Humm, "The CT motion quantitation of lung lesions and its impact on PET-measured SUVs," J. Nucl. Med. **45**, 1287–1292 (2004).

[15]J. J. Hamill, A. Dekker, and G. Bosmans, "Respiratory-gated CT as a tool for the simulation of breathing artifacts in PET and PET/CT," Abstract 539 at the Society of Nuclear Medicine 53rd Annual Meeting, 2006.

[16]X. A. Li, C. Stepaniak, and E. Gore, "Technical and dosimetric aspects of respiratory gating using a pressure-sensor motion monitoring system," Med. Phys. **33**, 145–154 (2006).

[17]J. P. J. Carney, D. W. Townsend, V. Rappoport, and B. Bendriem, Med. Phys. **33**, 976–983 (2006).

[18]J. Hamill, C. Michel, and P. Kinahan, "Fast PET EM reconstruction from linograms," IEEE Trans. Nucl. Sci. **50**, 1630–1635 (2003).

[19]H. H. Liu *et al.*, "Assessing respiration-induced tumor motion and internal target volume using four-dimensional computed tomography for radiotherapy of lung cancer," Int. J. Radiat. Oncol. Biol. Phys. **68**, 531–540 (2007).

[20]R. Leahy and C. Byrne, "Recent development in iterative image reconstruction for PET and SPECT," IEEE Trans. Med. Imaging **19**, 257–260 (2000).

[21]J. Hamill and T. Bruckbauer, "Iterative reconstruction methods for high-throughput PET tomographs," Phys. Med. Biol. **47**, 2627–2636 (2002).

[22]G. W. Goerres, E. Kamel, T. H. Heidelberg, M. R. Schwitter, C. Burger, and G. K. von Schulthess, "PET-CT image co-registration in the thorax: Influence of respiration," Eur. J. Nucl. Med. **29**, 351–360 (2002).

[23]G. W. Goerres, C. Burger, M. R. Schwitter, T. H. Heidelberg, B. Seifert, and G. K. von Schulthess, "PET/CT of the abdomen: Optimizing the patient breathing pattern," Eur. Radiol. **13**, 734–739 (2003).

[24]N. Koch, H. H. Liu, G. Starkschall, M. Jacobson, K. Forster, Z. Liao, R. Komaki, and C. W. Stevens, "Evaluation of internal lung motion for respiratory-gated radiotherapy using MRI: Part I—Correlating internal lung motion with skin fiducial motion," Int. J. Radiat. Oncol. Biol. Phys. **60**, 1459–1472 (2004).

[25]W. Lu, P. J. Parikh, J. P. Hubenschmidt, J. D. Bradley, and D. A. Low, "A comparison between amplitude sorting and phase-angle sorting using external respiratory measurement for 4D CT," Med. Phys. **33**, 2964–2974 (2006).

[26]J. Streeter, R. Eisner, J. Hamill, M. Nelson, and R. Patterson, "Attenuation correction of stress PET Rb82 with ultrafast CT images," Abstract 1729 at the Society of Nuclear Medicine 54th Annual Meeting, 2007.